JACS
JOURNAL OF THE AMERICAN CHEMICAL SOCIETY

Article

pubs.acs.org/JACS

Enhanced Thermal Decomposition of Nitromethane on Functionalized Graphene Sheets: Ab Initio Molecular Dynamics Simulations

Li-Min Liu,[†,‡] Roberto Car,[†] Annabella Selloni,[†,*] Daniel M. Dabbs,[§] Ilhan A. Aksay,[§] and Richard A. Yetter[∥]

[†]Department of Chemistry, Princeton University, Princeton, New Jersey 08544, United States

[‡]Beijing Computational Science Research Centre, Beijing 100084, China

[§]Department of Chemical and Biological Engineering, Princeton University, New Jersey 08544, United States

[∥]Department of Mechanical and Nuclear Engineering, The Pennsylvania State University, University Park, Pennsylvania 16802, United States

Supporting Information

ABSTRACT: The burning rate of the monopropellant nitromethane (NM) has been observed to increase by adding and dispersing small amounts of functionalized graphene sheets (FGSs) in liquid NM. Until now, no plausible mechanisms for FGSs acting as combustion catalysts have been presented. Here, we report ab initio molecular dynamics simulations showing that carbon vacancy defects within the plane of the FGSs, functionalized with oxygen-containing groups, greatly accelerate the thermal decomposition of NM and its derivatives. This occurs through reaction pathways involving the exchange of protons or oxygens between the oxygen-containing functional groups and NM and its derivatives. FGS initiates and promotes the decomposition of the monopropellant and its derivatives, ultimately forming H_2O, CO_2, and N_2. Concomitantly, oxygen-containing functional groups on the FGSs are consumed and regenerated without significantly changing the FGSs in accordance with experiments indicating that the FGSs are not consumed during combustion.

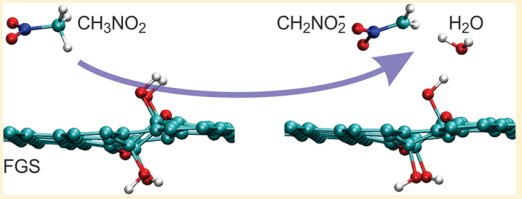

INTRODUCTION

Future high-speed propulsion systems will require environmentally friendly fuels that offer high energy density, short ignition times, and low costs.[1,2] It has been observed that small concentrations of nanoscale particles dispersed in a liquid fuel change the combustion properties of the fuel without significantly affecting its energetics, prompting research to find optimal nanoparticles for use in propulsion systems.[3] In this respect functionalized graphene sheets[4−6] (FGSs) are very promising as it was recently shown that dispersing them in liquid nitromethane (CH_3NO_2) can increase the burning rate of the monopropellant up to 175% over neat NM, outperforming more conventional additives such as aluminum monohydroxide and silica nanoparticles.[7] It was suggested that the functionalized graphene acts as a catalyst, but it was impossible to determine the mechanisms using existing experimental techniques. Using ab initio molecular dynamics (AIMD) simulations,[8] we now demonstrate that the catalytic activity originates from lattice defect complexes within the graphene sheet, notably vacancies functionalized with oxygen-containing groups such as hydroxyls, ethers, and carbonyls, and provide detailed mechanistic insight into the atomic-scale processes leading to complete NM decomposition.

Neat nitromethane undergoes a complex combustion process[9] that in the gas phase is initiated by unimolecular dissociation ($CH_3NO_2 \rightarrow CH_3 + NO_2$), an event with large activation energy (~251 kJ/mol).[10,11] This reaction is followed by conversion of NO_2 into NO, whereas the methyl radicals are either oxidized or abstract H to make CH_4. This stage is followed by the complete reduction of NO to N_2 accompanied by the formation of species such as CO, H_2O, H_2, and CO_2 with substantial energy release. Oxidation/reduction of NO, the primary intermediate product, is relatively slow and the transition from the first stage of dissociation to massive oxidation/reduction constitutes an intermediate dark zone characterized by a plateau in the reaction temperature. In the presence of a catalyst, different reaction pathways may become effective, as indicated by the occurrence of different reaction products and the notable absence of CH_4 suggesting that C−N bond breaking is not a prerequisite for heterogeneous reactions.[12] Formation of aci-ions, $CH_2NO_2^-$, was observed in the initial stage of NM decomposition on γ-alumina.[13] Experimental observations suggest that these ions play a crucial role in the detonation kinetics of dense NM.[14] Formation of aci-ions through a bimolecular mechanism also characterizes the onset of the pressure-induced reactions of neat NM at room-temperature.[15] Ab initio[16] and reactive field[17] MD

Received: June 15, 2012

   dx.doi.org/10.1021/ja3058277 | J. Am. Chem. Soc. XXXX, XXX, XXX−XXX

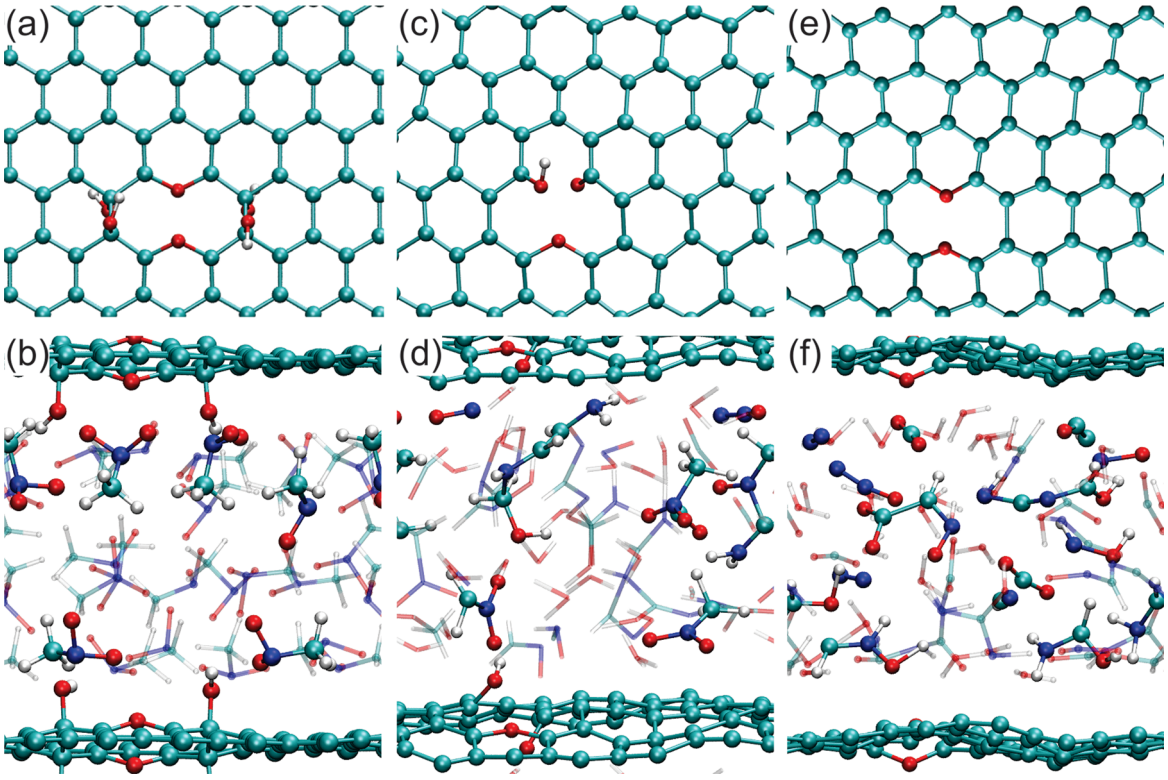

Figure 1. Atomic structures of FGS and nitromethane during the NM decomposition reaction. The schematics show the atomic structures of the FGS model (upper panels, top views) and FGS + liquid NM system (lower panels, side views) observed in our AIMD simulations: (a) and (b) initial configuration; (c) and (d) after 10 ps; (e) and (f) final configuration. In the lower panels, a few intermediates or decomposition products are highlighted. White, red, cyan, and blue balls (bonds) represent hydrogen, oxygen, carbon, and nitrogen atoms, respectively.

simulations show that in liquid NM at extreme density (ρ ~2000 kg/m^3) and temperature (T ~3000 K), proton exchange replaces C−N breaking in the initial stage of decomposition.

A good structural model is a prerequisite for investigating the role of FGS in NM combustion. In agreement with simple chemical intuition, our calculations show that pristine graphene interacts very weakly with NM, mostly via dispersion forces. Hydroxyl or epoxy groups adsorbed on graphene can form H-bonds with NM and abstract H from NM with significantly lower barriers than required for C−N bond scission. We show that while these processes facilitate NM decomposition they do not lead to catalytic action, as the outcome is just the desorption of the functional groups that results in inert graphene (Supporting Information). In fact, a model in which hydroxyls and epoxies are adsorbed on graphene is too simplistic as the FGSs used in our experimental studies are produced by strong chemical processes: massive oxidation to exfoliate and form graphene oxide sheets with nominal carbon to oxygen ratio (C/O) of 2 (FGS_2, where the subscript number designates the C/O), followed by thermal reduction to increase the C/O.[4−6,18−20] In the combustion experiments,[7] we used an FGS with a C/O of 22, FGS_{22}. The lateral dimensions of FGS are typically 100 nm to a few micrometers.[4,5] The thermal reduction of FGS_2 removes both C and O atoms creating carbon vacancies in the graphene network which are subsequently functionalized with ethers, hydroxyls, and carbonyls that saturate the sp^2 dangling bonds present at the vacancy edges.[4,5,21] Similar results were also reported in recent reactive field MD simulations of thermally reduced graphene oxide.[19] Additional hydroxyls or epoxies, if present, would tend to crowd in the vicinity of the decorated vacancy complexes. We show that it is these vacancy regions that play a major role in NM decomposition.

RESULTS AND DISCUSSION

The FGS model that we use in this study is depicted in Figure 1a: it contains a divacancy decorated by two ethers with 4 additional hydroxyls attached to C atoms nearby. The complex is embedded in a planar graphene sheet containing 60 atoms with periodic boundary conditions, for a C/O of 10. To gain insight into the effect of FGS on NM combustion, we periodically stack the FGSs with a separation of 13 Å between adjacent layers and fill the space in between with liquid NM (Figure 1b). We then perform AIMD simulations on the periodically repeated cell. Modeling combustion at the molecular scale is very challenging as this is a nonequilibrium process that occurs in a macroscopically highly inhomogeneous system consisting of the liquid fuel separated by a moving interface from the region of the flame where combustion takes place. The flame attains very high temperature, estimated at ~2400 K at steady state under the conditions of the experiment,[7] whereas the bulk liquid stays much cooler (the normal boiling point of NM is at 374 K). Combustion is expected to initiate at the interface featuring a large temperature gradient. Highly inhomogeneous macroscopic conditions are not meaningful at the microscopic scale of our simulated sample, which models a small molecular portion of NM and FGS in the interfacial region important for combustion. We thus adopt canonical particle number (N), volume (V), and temperature (T) (NVT) conditions with T ~2400 K and two density conditions: high (27 NM molecules),

dx.doi.org/10.1021/ja3058277 | J. Am. Chem. Soc. XXXX, XXX, XXX−XXX

ρ ~1900 kg/m^3, and low (20 NM molecules), with ρ ~1400 kg/m^3, respectively, in two separate runs. (The NM density was estimated by excluding the volume of the graphene sheet, which was taken as approximately equal to that of one layer of graphite.) More realistically, T and ρ should be lower, as T ~2400 K should be appropriate in the midst of the flame and the NM density at the experimental pressure (~5 MPa)[7] should not be significantly greater than the liquid density at standard temperature and pressure (STP) (ρ = 1137 kg/m^3). We will argue later that our choice of T and ρ has the main effect of accelerating the reactions without significantly affecting the catalytic mechanisms.

In AIMD, the potential energy surface for nuclear motion is generated on the fly from the instantaneous ground state of the electrons within Kohn–Sham DFT.[22] The latter is a widely used quantum chemical approach combining moderate computational cost and good predictive power. Here, we use DFT at the generalized gradient approximation (GGA) level with the parametrization of Perdew-Burke-Ernzerhorf (PBE),[23] which has been extensively tested and found to provide an overall satisfactory description of NM properties and decomposition processes in previous studies.[16,24−26] Detailed tests of our computational setup are presented in the Methods section (below) and the Supporting Information. Chemical reactions with low activation energies occur spontaneously in AIMD simulations making this approach very effective for the study of reactive chemical dynamics in condensed phase. In our first simulations, we included 27 NM molecules in the cell, corresponding to a density of ~1900 kg/m^3. The system was gradually heated to T~2400K and was then evolved at NVT for ~16 ps. Chemical reactions took place almost immediately leading to a rapid extinction of the initial NM population and the appearance of final products, mainly H_2O, CO_2, and N_2, as shown by the time evolution of the corresponding chemical species in Figure 2a. Remarkably, when suppressing the catalytic activity of FGS, no reactions took place in a time span of ~5 ps, as indicated by the curve marked frozen FGS in Figure 2a. These data refer to a run in which the initial conditions were the same as those of the longer simulation reported in the same figure. In the shorter (~5 ps) run, however, only the NM fluid was allowed to evolve at NVT, whereas FGS was kept frozen in its initial configuration, thus suppressing atomic exchanges with NM. The evolution of the aci-ion ($CH_2NO_2^-$) population is also shown in Figure 2a: this species is a reaction product that appears at the onset of the simulation and subsequently disappears within ~2 ps after extinction of the NM population, a behavior suggesting that NM decomposition is initiated by catalytic production of aci-ions.

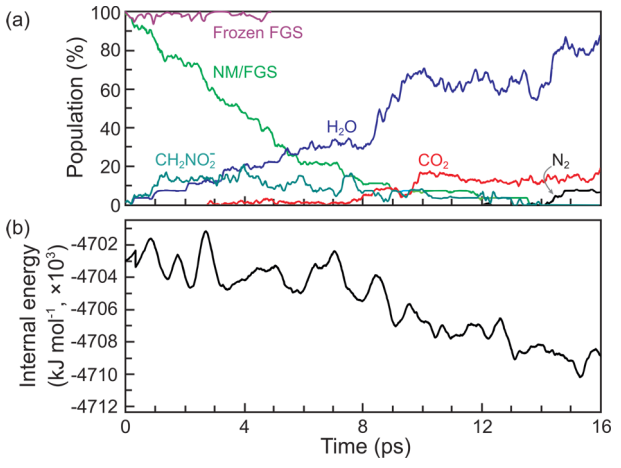

Figure 2. Reaction products formed from the decomposition of nitromethane. (a) Time evolution of the population of NM molecules and their main decomposition products (H_2O, CO_2, and N_2) during an AIMD simulation at T ~2400 K and a NM density of about ~1900 kg/m^3. For comparison, the population of pure NM in a simulation with the same conditions but where FGS is frozen in its initial configurations is also shown (purple line). (b) Time evolution of the internal energy in the same AIMD run.

The chemical reaction energetics is illustrated by the time evolution of the internal energy (sum of kinetic and potential energy) of the system reported in Figure 2b. As the system evolves at constant temperature, the drift of the internal energy depicts the evolution of the heat of reaction. We distinguish two regimes. During the first ~7 ps, the reactions are on average only moderately exothermic and exhibit large endothermic fluctuations, consistent with the activated nature of the events that initiate the combustion process. After ~7 ps the residual NM population is ~20% of the initial value (Figure 2a) and significant amounts of intermediate products are present. The evolution into final products is strongly exothermic as indicated by the rapid drop of the internal energy after 7 ps. Overall, the energy released is about 200 kJ per mole of NM.

It is instructive to monitor the evolution of FGS structure during combustion. Initially C/O is 10 and, after a phase of ~4 ps in which the hydroxyls (Figure 1a) are consumed, the divacancy complex settles in the configuration with C/O of 20 shown in Figure 1c, in which the sp^2 dangling bonds are saturated by a hydroxyl, a carbonyl, and an ether. The decrease of the number of oxygens on FGS is consistent with results of ab initio thermodynamics calculations showing that on average only 2−4 adsorbed oxygens should be present on the divacancy at the temperature and pressure of the simulation (ref 27 and Figure S2b of the Supporting Information). The configuration in Figure 1c is dynamically stable and lasts almost until the end of the simulation, that is, up to the disappearance of the last aci ion after ~14 ps have elapsed. During this time interval, FGS has a nominal C/O of 20 and the divacancy complex keeps exchanging protons with the reacting fluid. Typically, the hydroxyl converts to a carbonyl by donating a proton to an NM molecule or a reaction product, whereas the carbonyl converts to a hydroxyl by extracting a proton from an NM molecule or a reaction product. The carbonyl can also oxidize CH_2NO_2H into CH_2ONO_2H, leaving a dangling bond,[28] which then abstracts O from another CH_3NO_2 molecule so that a carbonyl is formed again. Uniquely, these processes drive a catalytic cycle that leaves the divacancy complex unchanged on average. Although isolated H and OH groups occasionally form on the defect-free graphene part of FGS, they quickly react with other species and their lifetime is very short. The complex flow of reactions can be summarized as follows. Initially FGS decomposes NM into species such as $CH_2NO_2^-$, CH_3NO, or $CH_3NO_2H^+$ that quickly undergo additional reactions. CH_2NO_2H is a typical intermediate, which can react either with an intact NM molecule, or with other intermediates, or with FGS (Figure 3). For instance, CH_2NO_2H can be oxidized to CH_2ONO_2H, which then decomposes into CH_2O and HNO_2. Alternatively, CH_2NO_2H can react with an OH group on FGS to form CH_2NO and water. CH_2NO is very reactive and can easily

dx.doi.org/10.1021/ja3058277 | J. Am. Chem. Soc. XXXX, XXX, XXX−XXX

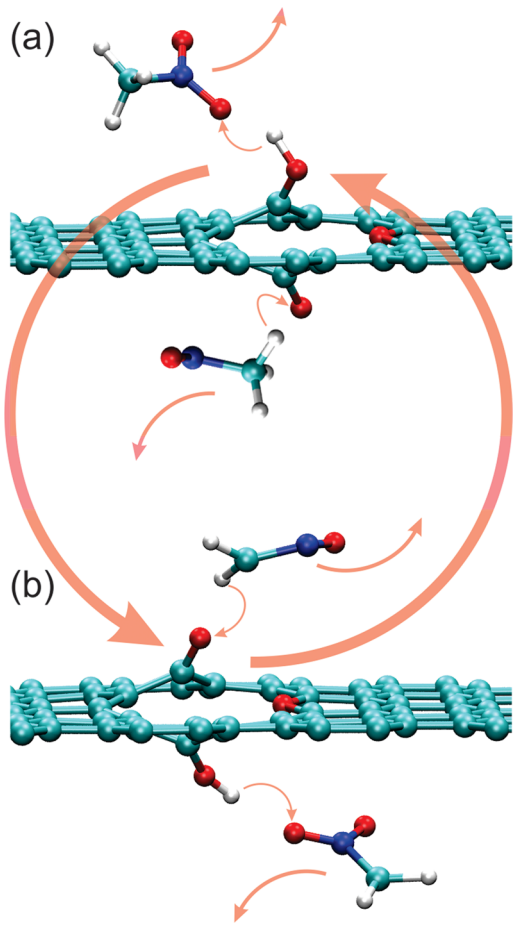

Figure 3. Catalytic role of the FGS in the decomposition reaction of nitromethane. (a) An example of a proton transfer from a hydroxyl group on an FGS to a nitromethane molecule forming a reactive intermediate. (b) The subsequent regeneration of the hydroxyl group caused by a proton transfer from (in this example) a nitromethane derivative to a carbonyl on the FGS. Other examples of proton transfer mechanisms are shown below the basal plane, representing a small sampling of the potential reactions occurring between FGS and nitromethane and FGS and NM derivatives.

capture O from NM or another intermediate to form CH_2ONO, which is unstable and decomposes into CH_2O and NO. CH_2O can be further oxidized to form CO or CO_2, with the release of water, the main product of the decomposition process. Protons are also frequently generated. A proton is generally bound to a water molecule forming a hydronium ion, H_3O^+, and can be rapidly transferred via the Grotthuss exchange mechanism[28] to another water molecule or to a different oxygen containing species contributing to the acceleration of the reactions. The catalytic role of FGS is essential to initiate the process and transform the NM molecules into more reactive intermediates. Once these are formed, reactions also start to proceed directly within the fluid. Overall, the decomposition is very fast. After ~14 ps, all the NMs transform into different species. The main combustion products are H_2O, CO_2, and N_2, consistent with previous studies of neat NM.[17,25,29] Whereas H_2O and CO_2 are generated mainly in the initial and intermediate stages, N_2 is generated in the very last stage of the simulation (after ~12 ps), when most of the oxygen atoms have been consumed by forming H_2O and CO_2. In the end, when no more protons are available for exchange, only two ethers remain at the divacancy, and a 4-atom C−N chain forms in the fluid (Figure 1c). A similar chain was also observed in a recent AIMD simulation of the thermal decomposition of solid NM.[25] The decrease of the number of adsorbed oxygens at the divacancy in the final stages of the simulation is consistent with the fact that neat NM does not contain sufficient oxygen for complete combustion.[7]

Lowering the density to ρ~1400 kg/m^3 reduces the NM molecules initially present in the cell from 27 to 20, but does not change qualitatively the combustion process. This is still initiated by protonation, deprotonation and oxidation reactions promoted by FGS. The lower liquid density, however, slows down the entire process as discussed in more detail in the Supporting Information. In particular, we observe a reduction of the rate of catalyzed reactions, which is roughly proportional to the density reduction, as expected. Given the endothermic character of the initial decomposition reactions, lowering the temperature should reduce the burning rate more dramatically. In view of the limited time span accessible to AIMD, we have not attempted simulations at lower temperatures. The use of a statistical approach to sample the free energy surface, such as, for example, metadynamics,[30] which does not necessitate a priori knowledge of the final state of the system, would require the identification of suitable reaction coordinates, which is hardly feasible for a complex system such as the one of interest, with a very large number of possible reactions and pathways. We notice, however, that at lower temperatures, FGS should play an even more prominent role in initiating the combustion as the heterogeneous reactions promoted by FGS have significantly lower activation energy than the alternative homogeneous reactions. To obtain a simple estimate of this effect, we determined the energy barrier for the initial reaction of a NM molecule with a hydroxyl group on FGS to form $CH_2NO_2^-$ and water (Supporting Information). The resulting value, 121 kJ/mol, can be compared to, for example, the effective activation energy for the initial stages of neat NM decomposition, E_{a1} ~206 kJ/mol, found in recent reactive force field simulations.[29] The difference of ~85 kJ/mol suggests that the probability of the heterogeneous reaction should increase by a factor of nearly 10^2 relative to the homogeneous one when the temperature is reduced from 2400 to, for example 1200 K. As a matter of fact, facile decomposition of NM has been observed on various solid surfaces at relatively low temperatures and pressures,[12,13] that is, under conditions where neat NM is not reactive, indicating that the heterogeneous decomposition mechanism becomes indeed increasingly favored with decreasing temperature.

In conclusion, we have demonstrated that graphene with carbon vacancies is an effective catalyst for NM combustion. The key result is the difference between the curves labeled NM/FGS and Frozen FGS in Figure 2a. This clearly shows that FGS initiates the NM decomposition and strongly enhances the rate of successive reactions, in good agreement with experimental observations.[7] This property, in conjunction with excellent dispersive and thermal characteristics,[31,32] makes FGS a highly performing additive for future propulsion systems. The basic mechanisms by which FGS promotes NM combustion are associated with the highly defective regions, which form in FGS during thermal reduction of graphene oxide. The defect complexes consist of C vacancy clusters decorated by functional groups, such as hydroxyls and carbonyls, and can be viewed as internal edges within graphene. The divacancy considered here is just one of the simplest of these defect complexes, the concentration of which depends on

dx.doi.org/10.1021/ja3058277 | J. Am. Chem. Soc. XXXX, XXX, XXX−XXX

the extent of the thermal reduction process. The concentration increases with increasing C/O provided that the reduction temperature is low enough to minimize thermal annealing of the vacancies.[33] Thus, we should expect enhanced catalytic activity from FGS additives with larger C/O ratio.

METHODS

The DFT calculations used the PBE[23] exchange-correlation functional and norm conserving Goedecker, Teter, and Hutter (GTH) pseudopotentials.[34] The CP2K/Quickstep[35] code was employed, which uses a hybrid Gaussian and plane wave basis set. The valence orbitals were expanded in Gaussian functions at the optimized double-ζ basis set level including diffusion terms. A plane wave cutoff of 320 Ry was used in the plane wave expansion of the electron density.

To test the accuracy of our computational setup, we performed calculations of the molecular properties of NM in gas phase. Geometric parameters, vibrational frequencies and relative stabilities of a few low energy isomers are compared to experiment and other computational results in Tables S1−S3 of the Supporting Information, respectively. Deviations of our computed structural parameters from experiment do not exceed 0.015 Å and 1.2 deg for bond lengths and bond angles, respectively. For vibrational frequencies, the largest deviation from experiment is 40 cm^{-1}. For the energies of methyl nitrite (CH_3ONO) and aci-nitromethane (CH_2NOOH) relative to nitromethane, the values given by our calculations are ∼3 kcal/mol higher and∼ 0.5 kcal/mol lower respectively in comparison to results of higher level calculations.[10,11]

The AIMD simulations were performed within the canonical (NVT) ensemble following the Born−Oppenheimer (BO) implementation.[35] The ionic equations of motion were integrated using the velocity Verlet algorithm with a time step of 1.0 fs; deuterium masses were used for the hydrogen atoms in order to enable a larger time step. The simulated system was initially equilibrated at a temperature of 300 K, which was then gradually increased at increments of 300 K followed by ∼1 ps time laps for equilibration. Finally, the system was left to evolve at 2400 K for ∼16 ps.

All products in Figure 2a were identified by their bond lengths and bond angles and the number of each product was calculated at each step. In particular, CO_2 was identified by requiring that one carbon binds to two O atoms (C−O distance <1.3 Å) and that there is no hydrogen within 1.2 Å of the C, so as to exclude HCOO. For H_2O, we required that one oxygen forms bonds with *exactly* two hydrogens (O−H distance <1.25 Å). For N_2, we required the N−N distance to be smaller than 1.25 Å, with no oxygen within 1.4 Å of either N, so as to exclude N_2O.

ASSOCIATED CONTENT

Supporting Information

Molecular properties of NM to test accuracy of the computational setup, energetics of the interaction of an NM molecule with graphene, ab initio thermodynamics calculations of the stability diagram of an oxidized divacancy, effect of NM density on its decomposition on an FGS, total energies and atomic coordinates of molecular NM isomers. Also included are two animations to better illustrate the dynamic and complex nature of the NM-FGS interactions near an FGS vacancy site under the conditions described in this article. This material is available free of charge via the Internet at http://pubs.acs.org.

AUTHOR INFORMATION

Corresponding Author

*E-mail: aselloni@Princeton.EDU.

Notes

The authors declare no competing financial interests.

ACKNOWLEDGMENTS

Financial support for this work was provided by the American Recovery and Reinvestment Act (ARRA) through the U.S. Air Force Office of Scientific Research (AFOSR) under Grant No. FA9550-09-1-0523. L.M.L. acknowledges also support from NSFC (No. 51222212 and 11244001).

REFERENCES

(1) Edwards, T. *J. Propul. Power* **2003**, *19*, 1089.
(2) Maurice, L. Q.; Lander, H.; Edwards, T.; Harrison, W. E. *Fuel* **2001**, *80*, 747.
(3) Wickham, D. T.; Cook, R.; De Voss, S.; Engel, J. R.; Nabity, J. *J. Russ. Laser Res.* **2006**, *27*, 552.
(4) Schniepp, H. C.; Li, J. L.; McAllister, M. J.; Sai, H.; Herrera-Alonso, M.; Adamson, D. H.; Prud'homme, R. K.; Car, R.; Saville, D. A.; Aksay, I. A. *J. Phys. Chem. B* **2006**, *110*, 8535.
(5) McAllister, M. J.; Li, J. L.; Adamson, D. H.; Schniepp, H. C.; Abdala, A. A.; Liu, J.; Herrera-Alonso, M.; Milius, D. L.; Car, R.; Prud'homme, R. K.; Aksay, I. A. *Chem. Mater.* **2007**, *19*, 4396.
(6) Park, S.; Ruoff, R. S. *Nature Nanotechnol.* **2009**, *4*, 217.
(7) Sabourin, J. L.; Dabbs, D. M.; Yetter, R. A.; Dryer, F. L.; Aksay, I. A. *ACS Nano* **2009**, *3*, 3945.
(8) Car, R.; Parrinello, M. *Phys. Rev. Lett.* **1985**, *55*, 2471.
(9) Melius, C. F. *J. Phys. IV* **1995**, *5*, 535.
(10) Asatryan, R.; Bozzelli, J. W.; Simmie, J. M. *J. Phys. Chem. A* **2008**, *112*, 3172.
(11) Hu, W.-F.; He, T.-J.; Chen, D.-M.; Liu, F.-C. *J. Phys. Chem. A* **2002**, *106*, 7294.
(12) Benziger, J. B. *Combust. Sci. Technol.* **1982**, *29*, 191.
(13) Yamaguchi, M. *J. Chem. Soc. Faraday Trans.* **1997**, *93*, 3581.
(14) Engelke, R.; Earl, W. L.; Rohlfing, C. M. *J. Chem. Phys.* **1986**, *84*, 142.
(15) Citroni, M.; Bini, R.; Pagliai, M.; Cardini, G.; Schettino, V. *J. Phys. Chem. B* **2010**, *114*, 9420.
(16) Manaa, M. R.; Reed, E. J.; Fried, L. E.; Galli, G.; Gygi, F. *J. Chem. Phys.* **2004**, *120*, 10146.
(17) Han, S. P.; van Duin, A. C. T.; Goddard, W. A.; Strachan, A. *J. Phys. Chem. B* **2011**, *115*, 6534.
(18) Compton, O. C.; Nguyen, S. T. *Small* **2010**, *6*, 711.
(19) Bagri, A.; Mattevi, C.; Acik, M.; Chabal, Y. J.; Chhowalla, M.; Shenoy, V. B. *Nat. Chem.* **2010**, *2*, 581.
(20) Gao, W.; Alemany, L. B.; Ci, L. J.; Ajayan, P. M. *Nat. Chem.* **2009**, *1*, 403.
(21) Kudin, K. N.; Ozbas, B.; Schniepp, H. C.; Prud'homme, R. K.; Aksay, I. A.; Car, R. *Nano Lett.* **2008**, *8*, 36.
(22) Kohn, W.; Sham, L. *Phys. Rev.* **1965**, *140*, A1133.
(23) Perdew, J. P.; Burke, K.; Ernzerhof, M. *Phys. Rev. Lett.* **1996**, *77*, 3865.
(24) Liu, H.; Zhao, J.; Wei, D.; Gong, Z. *J. Chem. Phys.* **2006**, *124*, 124501.
(25) Chang, J.; Lian, P.; Wei, D. Q.; Chen, X. R.; Zhang, Q. M.; Gong, Z. Z. *Phys. Rev. Lett.* **2010**, 105.
(26) NIST *Chemistry WebBook: Computational Chemistry Comparison and Benchmark Database (http://cccbdb.nist.gov/)* 2011.
(27) Carlsson, J. M.; Hanke, F.; Linic, S.; Scheffler, M. *Phys. Rev. Lett.* **2009**, *102*.
(28) Marx, D. *ChemPhysChem.* **2006**, *7*, 1848.
(29) Rom, N.; Zybin, S. V.; van Duin, A. C. T.; Goddard, W. A.; Zeiri, Y.; Katz, G.; Kosloff, R. *J. Phys. Chem. A* **2011**, *115*, 10181.
(30) Laio, A.; Parrinello, M. *Proc. Natl. Acad. Sci. U. S. A.* **2002**, *99*, 12562.

(31) Balandin, A. A.; Ghosh, S.; Bao, W. Z.; Calizo, I.; Teweldebrhan, D.; Miao, F.; Lau, C. N. *Nano Lett.* **2008**, *8*, 902.
(32) Balandin, A. A. *Nat. Mater.* **2011**, *10*, 569.
(33) Sato, K.; Saito, R.; Oyama, Y.; Jian, J.; Cancado, L. G.; Pimenta, M. A.; Jorio, A.; Samsonidze, G. G.; Dresselhaus, G.; Dresselhaus, M. S. *Chem. Phys. Lett.* **2006**, *427*, 117.
(34) Goedecker, S.; Teter, M.; Hutter, J. *Phys. Rev. B* **1996**, *54*, 1703.
(35) VandeVondele, J.; Krack, M.; Mohamed, F.; Parrinello, M.; Chassaing, T.; Hutter, J. *Comput. Phys. Commun.* **2005**, *167*, 103.